IEEE Access
Multidisciplinary | Rapid Review | Open Access Journal

Received July 14, 2020, accepted August 1, 2020, date of publication August 11, 2020, date of current version August 24, 2020.

Digital Object Identifier 10.1109/ACCESS.2020.3015741

Enabling Multiple Power Beacons for Uplink of NOMA-Enabled Mobile Edge Computing in Wirelessly Powered IoT

DINH-THUAN DO[1], (Senior Member, IEEE), MINH-SANG VAN NGUYEN[2], TU N. NGUYEN[3], (Senior Member, IEEE), XINGWANG LI[4], (Senior Member, IEEE), AND KWONHUE CHOI[5]

[1]Department of Computer Science and Information Engineering, College of Information and Electrical Engineering, Asia University, Taichung City 41354, Taiwan
[2]Faculty of Electronics Technology, Industrial University of Ho Chi Minh City (IUH), Ho Chi Minh City 700000, Vietnam
[3]Department of Computer Science, Purdue University Fort Wayne, Fort Wayne, IN 48835, USA
[4]School of Physical and Electronics Engineering, Henan Polytechnic University, Jiaozuo 454000, China
[5]Department of Information and Communication Engineering, Yeungnam University, Gyeongsan 38541, South Korea

Corresponding authors: Dinh-Thuan Do (dodinhthuan@asia.edu.tw) and Kwonhue Choi (gonew@ynu.ac.kr)

This work was supported in part by the National Research Foundation of Korea (NRF) through the Brain Korea 21 Plus Program under Grant 22A20130012814, and in part by the 2019 Yeungnam University Research Grant.

ABSTRACT As a promising technique, power beacon provides ability of wireless energy transfer to relaying devices in Internet of Things (IoT) to serve far devices with respect to low latency and high spectrum efficiency manner. Mobile edge computing (MEC) enables smart devices to offload parts of their computation-workloads to the cellular base stations associated with edge servers. This paper introduces a promising multiple access technique, namely non-orthogonal multiple access (NOMA) to provide communication service between the base station associated with MEC and far IoT devices. In this paper, we indicate that the multiple power beacons (PBs) benefits to uplink of NOMA-MEC system with the wireless powered IoT. More antennas equipped at smart device and more PBs exhibit reasonable outage performance for the considered system. The simulation results reveal in two folds: (1) *our proposed scheme can simultaneously achieve higher spectrum efficiency and ensure prolong lifetime of IoT devices*; (2) *the mobility of relay leads to select PB appropriately and hence the suitable scheme is realized as comparing two schemes related to ability of energy harvesting and acceptable outage behavior.*

INDEX TERMS Power beacon, NOMA, outage probability, mobile edge computing.

I. INTRODUCTION

Due to capability of connecting heterogeneous devices, the IoT has attracted increased attention [1]. IoT can be implemented with wide range of technologies and applications through device to device (D2D) and cellular wireless communications [2]. Conventional IoT terminals or smart devices are limited in term of computation-resources, and poor resource leads to the degraded quality of experience (e.g., a long computational delay) since the resource-hungry services are required. To overcome such difficulty, mobile edge computing (MEC) allows smart devices to actively offload parts of their computation-workloads to the edge servers associated with cellular base stations [3], [4]. The authors in [5] introduced scheme enabling the IoT device to optimize the offloading policy without three terms including the energy consumption model, knowledge of the MEC model and the computation latency model. Integrating MEC with wireless power transfer is a promising technique in the IoT network introduced in [6]. IoT together with applications provides the better communication quality services for the fifth generation (5G) [7] and beyond 5G (B5G) [8]–[10]. These investigations are developed to satisfy demand in both the academia and the industry in recent years. IoT will play an irreplaceable role and it is benefited from the advantages and the development of the IoT systems. For example, applications of IoT are

The associate editor coordinating the review of this manuscript and approving it for publication was Tie Qiu.

introduced for 5G and B5G systems [11]–[13]. Meanwhile, two major problems of the IoT need be urgently addressed. Firstly, limitation of the spectrum resources occurs since the widespread deployment of the IoT devices. Secondly, it is a critical problem of power consumption and prolonging the lifetime of the IoT since most of the devices are battery powered constraint. Fortunately, several effective technologies in terms of spectrum sharing and power control have been developed in order to address these problems. For the cellular IoT, NOMA is proposed due to higher spectrum efficiency. NOMA provides an innovative access scheme to accommodate multiple users. These multiple users can be shared on the same frequency (or time) through successive interference cancellation (SIC) technology [14]–[16].

A. RELATED WORK

Regarding implementing wireless power transfer to green networks, the base station provides energy to devices and support to transmit information for uplink communication by using NOMA as recent work [17], [18]. A similar study for a wireless-powered sensor network was conducted in [19]. The authors in [20] studied a NOMA based heterogeneous network to consider the trade-off among harvested energy, sum rate, the energy efficiency and fairness. A cognitive radio-assisted NOMA networks are presented by evaluating optimal resource allocation strategies as in [21]. The machine-to-machine communication benefits from wireless power transfer technique and NOMA scheme. In such network, the machine-type communication device is able to harvest energy in the downlink while the uplink transmitting information to the base station via machine-type communication gateway as in [22], [23]. It is not simultaneous implementation of energy harvesting and information detection since these works studied problems for single antenna nodes which either harvest energy or decode information. In cooperative NOMA systems relying energy harvesting [24]–[26], the cell-centered users harvest energy from the base station based on the wireless received signals. These harvesting users play role as a relay to forward the information to the cell-edge users (far users). Most of works used power splitting based energy harvesting at the relay users. For example, the authors in [30]–[33] derived expressions of outage probability for far users.

B. OUR CONTRIBUTION

However, above works only focus on the outage improvement in relaying networks, even in condition of energy-constrained users which are deployed to forward signal to far users, while neglect the ability of energy harvesting from the beacons [24]–[26]. In other challenging work, secure performance is considered in the situation of IoT using multiple power beacons (PBs) in the presence of a passive eavesdropper, which is very advantageous for energy constrained IoT devices [34]. However, when the harvested energy is applied in the energy-constrained devices in challenging network, i.e. such as NOMA-MEC, is insufficient, the system meets worse performance since it cannot assist the NOMA transmission, i.e., outage performance need be evaluated. Therefore, it is necessary to ensure the data transmission with higher reliability of for wireless powered IoT devices in energy-efficient way.

According to the literature reviews above, though there are lots of work considering both energy harvesting and NOMA-enabled MEC network, the research on outage performance for such network can still be further improved. Therefore, considering uplink of NOMA-MEC network under help of multiple PBs, namely a beacon-assisted NOMA-MEC system is proposed in this paper to improve energy shorten existing in IoT applications. On one hand, different from the traditional NOMA network, beacon-assisted NOMA-MEC can achieve low outage probability compared with orthogonal multiple access (OMA). Furthermore, this proposed system can achieve the best trade-off between information and lifetime for energy-limited wireless networks. The contributions of this article are summarized as follows:

- We consider multiple PBs and relay scheme to serve NOMA-MEC transmission in main links, where the best PB is selected by the relay. Compared with the OMA scheme and the NOMA-MEC scheme is able to fully utilize the power transfer channels contributed by multiple PBs.
- We derive the closed-form expressions of the outage probability for evaluating ability of wireless power transfer from best power beacon to serve far IoT devices for signal transmission in uplink. Simulation results demonstrate performance gap of two MEC devices in term of outage probability related with higher number of transmit antennas and higher number of beacons.
- This system benefits from multiple antennas architecture, i.e. by increasing the number of antennas and power beacons the outage performance can be improved significantly. Furthermore, simulation results indicated that the outage performance of the proposed scheme is slightly better than that of the OMA-MEC model.

The rest of this paper is organized as follows. Section II describes the NOMA-MEC system in two scenarios related to capability of energy harvesting. In Section III, we consider the scenario of energy harvesting which is enabled at relay. Section IV extends our works to the scenario of two nodes are able to harvest energy. Similarly, we analyze the outage performance of OMA-MEC system. We conduct extensive simulations in Section VI, and Section VII concludes the paper.

Notation: Throughout this paper, $\Pr(.)$ denotes probability, $F_Z(.)$ and $f_Z(.)$ symbolize the cumulative distribution function (CDF) and the probability density function (PDF) of a random variable Z, respectively, and $K_1\{.\}$ is the first order modified Bessel function of the second kind.

II. SYSTEM MODEL

We consider as illustration in Fig. 1 and Fig. 2 corresponding two cases: (i) only relay harvests wireless energy, (ii) both

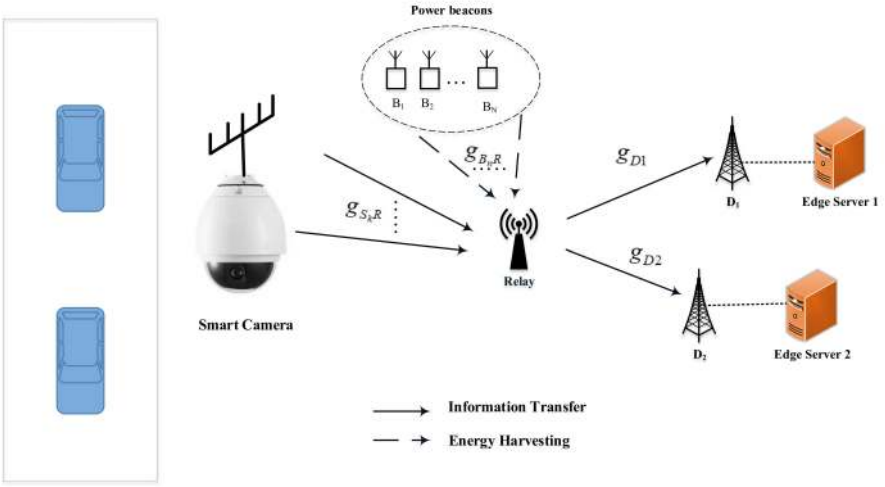

FIGURE 1. Scheme 1: Enabling energy harvesting at the relay *R*.

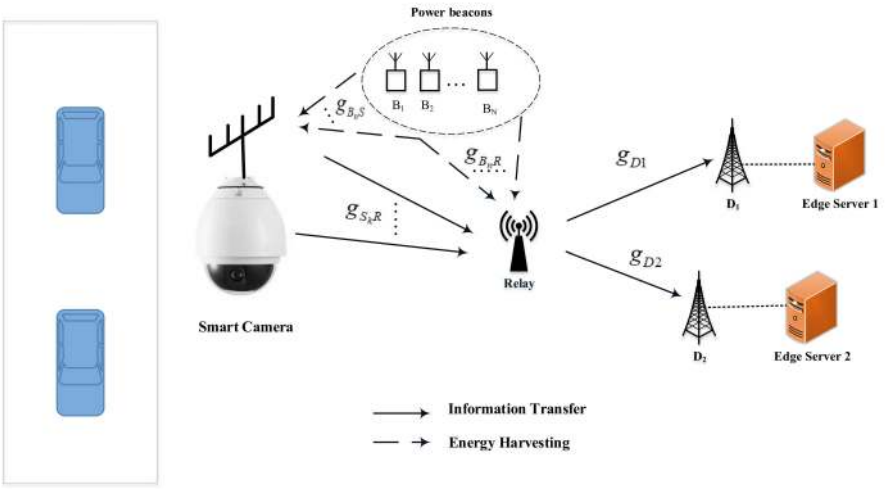

FIGURE 2. Scheme 2: Enabling energy harvesting at both the mart camera and the relay.

the smart camera (denoted as S) and relay R are able harvest energy. In particular, we study a uplink of cooperative NOMA network with one multiple antenna smart camera which intends to communicate with two edge servers (associated with base stations) D_1, D_2. In the second scenario of IoT network, the smart camera and the relay are power-constraint devices and they need help of N power beacons (denoted as PB) $B_1, B_2, \ldots, B_N$. It is assumed that the these PBs are clustered relatively closely together such that they have equivalent distances to the relay. Therefore, the channel gains between the PBs and the relay are independent identically distributed (i.i.d.), as commonly assumed in the related existing work [36]. It is noted that the main parameters are shown in Table 1.

In the first scenario, only power-constraint relay R is able to harvest wireless energy from the group of PBs. This assumption is reasonable for IoT networks which contain equipment (sensors, relays) everywhere. Here, PB selection is adopted as in [34].[1] In this system model, each node is facilitated with single antenna, except for the S. Due to deep fading, it is assumed that the direct links do not exist between the S and two MEC devices.[2] In Scheme 1, the S communicates with the distant base stations in the uplink with the assistance of the relay under ability of energy harvesting. In Scheme 2, both the smart camera S and the relay R are equipped with small batteries for energy storage due to the size and cost limitations. The camera S sends the superimposed signals x_1, x_2 dedicated to two MEC devices. The two signals x_1, x_2

[1] Although, the non-linear energy harvester is adopted as in [26]–[29], however multiple beacons allow system a chance to achieve improved performance. In non-linear energy harvester, the amount of harvested energy depends on the saturated threshold at the harvester. We also extend to case of non-linear energy harvester in future.

[2] Our work can be easily extended to multiple user scenario or as our future work.

TABLE 1. Key parameters of the system model.

Symbol	Description
x_i	the information symbol dedicated to Di, $(i = 1, 2)$
a_i	the power allocation coefficient for x_i
n	the index of PB, $n = 1, 2..., N$
k	the index of antenna at the camera, $k = 1, 2..., K$
R_i	the target rate to decode signal x_i
P_S	the transmit power of S
P_R	the transmit power of R
P_B	the transmit power of the selected power beacon
ω_R	the AWGN at R with $\omega_R \sim CN(0, N_0)$
ω_{D_i}	the AWGN at D_i with $\omega_{D_i} \sim CN(0, N_0)$
α	the time fraction that depends on the schedule of the power beacon with $(0 < \alpha < 1)$
τ	the efficiency coefficient of the energy conversion process with $(0 < \tau < 1)$
$g_{S_k R}$	the Rayleigh fading channel coefficients of $S \rightarrow R$ with $\left\|g_{S_k R}\right\|^2 \sim CN(0, \lambda_{SR}), (k = 1, \ldots, K)$
$g_{B_n S}$	the Rayleigh fading channel coefficients of $B \rightarrow S$ with $\left\|g_{B_n S}\right\|^2 \sim CN(0, \lambda_S), (n = 1, \ldots, N)$
$g_{B_n R}$	the Rayleigh fading channel coefficients of $B \rightarrow R$ with $\left\|g_{B_n R}\right\|^2 \sim CN(0, \lambda_{BR})$
g_{D_1}	the Rayleigh fading channel coefficients of $R \rightarrow D_1$ with $\left\|g_{D_1}\right\|^2 \sim CN(0, \lambda_{D1})$
g_{D_2}	the Rayleigh fading channel coefficients of $R \rightarrow D_2$ with $\left\|g_{D_2}\right\|^2 \sim CN(0, \lambda_{D2})$
$\bar{g}_{S_k R}$	the Rayleigh fading channel coefficients at R associated with imperfect SIC $\bar{g}_{S_k R} \sim CN(0, \eta\lambda_{SRip})$
η	the level of residual interference caused by imperfect SIC with $(0 \leq \eta \leq 1)$
$\bar{g}_{D_2}$	the Rayleigh fading channel coefficients at R with $\bar{g}_{D_2} \sim CN(0, \eta\lambda_{D2ip})$

are allocated corresponding power allocation factors a_1, a_2, respectively.

In the first phase, the received signal at the link $S \rightarrow R$ is given by

$$y_{S-R} = \sqrt{P_S} g_{S_k R} \left(\sqrt{a_1} x_1 + \sqrt{a_2} x_2\right) + \omega_R, \tag{1}$$

where $a_1 + a_2 = 1$ and without loss of generality, it is assumed that $a_1 > a_2$.

Based on the decoding principle of NOMA, the relay R decodes signal x_1 by treating the second base station's signal x_2 as noise. Hence, the signal to interference plus noise ratio (SINR) to decode x_1 at R is given by

$$\gamma_{S_k R - x_1} = \frac{a_1 P_S \left|g_{S_k R}\right|^2}{a_2 P_S \left|g_{S_k R}\right|^2 + N_0}. \tag{2}$$

After performing SIC, the SINR to decode x_2 at R is expressed as

$$\gamma_{S_k R - x_2} = \frac{a_2 P_S \left|g_{S_k R}\right|^2}{N_0}. \tag{3}$$

The decoded and re-encoded symbols are then further processed in the second phase. In particular, R forwards the re-encoded symbols to expected base stations in the uplink. The received signals at D_i are given by

$$y_{R-D_i} = \sqrt{P_R} g_{D_i} \left(\sqrt{a_1} x_1 + \sqrt{a_2} x_2\right) + \omega_{D_i}. \tag{4}$$

The SINR to decode x_1 at D_1 is given by

$$\gamma_{D_1 - x_1} = \frac{a_1 P_R \left|g_{D_1}\right|^2}{a_2 P_R \left|g_{D_1}\right|^2 + N_0}. \tag{5}$$

The SINR to decode x_1 at D_2 is given by

$$\gamma_{D_2 - x_1} = \frac{a_1 P_R \left|g_{D_2}\right|^2}{a_2 P_R \left|g_{D_2}\right|^2 + N_0}. \tag{6}$$

Similarly, SIC is required at the destinations, the SINR to decode x_2 at D_2 is formulated by

$$\gamma_{D_2 - x_2} = \frac{a_2 P_R \left|g_{D_2}\right|^2}{N_0}. \tag{7}$$

According to the transmit antenna section strategy, the camera S selects the antenna with the maximum quality of corresponding link to forward the message to the relay. Then, it can be acquired the diversity gain. It is noted that selection of best antenna by the source based on feedback of the CSI of link from the camera S to relay. In particular, to strengthen signal transmission of link $S \rightarrow R$ link, the antenna index can be selected at the camera as [37]

$$k^* = \arg \underbrace{\max}_{k=1,\ldots,K} \left(\left|g_{S_k R}\right|^2\right). \tag{8}$$

The selected PB with index n^* is required to strengthen link from group of PBs to relay as [3]

$$n^* = \arg \underbrace{\max}_{n=1,\ldots,N} \left(\left|g_{B_n R}\right|^2\right). \tag{9}$$

From (8) and (9), the CDF and the PDF related selected channel are given respectively by

$$F_{|g_{Z*R}|^2}(x) = 1 - \sum_{k=1}^{K} \binom{K}{k} (-1)^{k-1} \exp\left(-\frac{kx}{\lambda_{ZR}}\right), \tag{10}$$

where $(Z = \{S_k, B_n\})$, and

$$f_{|g_{Z*R}|^2}(x) = \sum_{k=1}^{K} \binom{K}{k} (-1)^{k-1} \frac{k}{\lambda_{ZR}} \exp\left(-\frac{kx}{\lambda_{ZR}}\right). \tag{11}$$

III. SCHEME 1: ENERGY HARVESTING AT THE RELAY

In the considered system, the relay R harvests energy from PB, and then such harvested energy is reused to transmit signals to far users. To robust wireless power transfer, the best PB in the considered system is selected to improve capability of energy harvesting from PB to the relay R. In addition, we assume that the time switching based energy harvesting technique is applied thanks to its high throughput [38]. It is denoted T as a transmission block time and R uses a duration of αT to harvest energy from the selected PB. Therefore, the energy harvested at the relay R is formulated by [38]

$$E_R = \tau P_B \alpha T \left|g_{B_{n*}R}\right|^2, \tag{12}$$

[3] In this scenario, the same power P_B is assigned to each PB. In principle, only one PB is selected to active ability of wireless power transfer while other PBs keep silent. The main advantage is the fact that PB selection is an energy-efficient wireless power transfer solution and hence the computational complexity can be reduced.

where $\left|g_{B_{n*}R}\right|^2$ is channel power gains of the links from the chosen *PB* $n*$ at link from group of power beacon to the relay. It is noted that optimizing problem of α is out of the scope of this paper. Under the assumption that the processing energy at R is negligible, the transmit power of R is written as [38]

$$P_R = \frac{2\tau P_B \alpha \left|g_{B_{n*}R}\right|^2}{(1-\alpha)} = \xi \left|g_{B_{n*}R}\right|^2, \tag{13}$$

where $\xi = \frac{2\tau P_B \alpha}{(1-\alpha)}$.

A. OUTAGE PERFORMANCE ANALYSIS

An outage event at each user occurs since the SINR during the first and second phases less than the target SINR υ_i. Due to the difference in their power allocation coefficients, it is pertinent to note that an outage behavior at D_1 is different from an outage behavior at D_2. As a result, the following subsections present the outage probability at D_1, D_2 separately.

1) OUTAGE ANALYSIS AT D_1

To consider outage performance of user D_1, we compute outage event based on ability of signal detection at related devices R and D_1 as below [39]

$$\begin{aligned} OP_1^{SC1} &= \Pr\left(\min\left(\gamma_{S_{k*}R-x_1}, \gamma_{D_1-x_1}\right) < \upsilon_1\right) \\ &= 1 - \Pr\left(\gamma_{S_{k*}R-x_1} > \upsilon_1, \gamma_{D_1-x_1} > \upsilon_1\right) \\ &= 1 - \underbrace{\Pr\left(\gamma_{S_{k*}R-x_1} > \upsilon_1\right)}_{\partial_1^{SC1}} \times \underbrace{\Pr\left(\gamma_{D_1-x_1} > \upsilon_1\right)}_{\partial_2^{SC1}}, \end{aligned} \tag{14}$$

where $\upsilon_i = 2^{2R_i} - 1$ and $R_i, i = 1, 2$ are target rates of user D_i.

Proposition 1: The closed-form expression of outage probability at D_1 in Scheme 1 is given as

$$\begin{aligned} OP_1^{SC1} &= 1 - \sum_{k=1}^{K} \binom{K}{k} (-1)^{k-1} \\ &\quad \times \exp\left(-\frac{k\upsilon_1 N_0}{P_{BS}\left(a_1 - \upsilon_1 a_2\right)\lambda_{SR}}\right) \\ &\quad \times \sum_{n=1}^{N} \binom{N}{n} (-1)^{n-1} \sqrt{\frac{4n\upsilon_1 N_0}{\xi\left(a_1 - \upsilon_1 a_2\right)\lambda_{BR}\lambda_{D1}}} \\ &\quad \times K_1\left(\sqrt{\frac{4n\upsilon_1 N_0}{\xi\left(a_1 - \upsilon_1 a_2\right)\lambda_{BR}\lambda_{D1}}}\right). \end{aligned} \tag{15}$$

Proof: See Appendix A.

Remark 1: Although the outage probability expression given in (15) can be readily evaluated through main parameters such as the number of antennas, transmit SNR at source, it is desirable to obtain reasonable outage probabilities for practical implementation. The antenna selection technique benefits to such outage performance, however we do not rely on this to reduce the computational complexity and cost of hardware design. For other confirmation, in the next subsections, we can be seen very tight matching between mathematical expressions results and simulation based results in the entire SNR range.

2) OUTAGE ANALYSIS AT D_2 WITH PERFECT SIC

Different with capability of signal detection at D_1, SIC is employed at D_2. Therefore, such outage probability at D_2 depends on how well SIC works to eliminate signal x_1 before detecting signal x_2. In case of perfect SIC, the outage probability is formulated as

$$\begin{aligned} OP_2^{SC1} &= \Pr\left(\min\left(\gamma_{S_{k*}R-x_2}, \gamma_{D_2-x_1}, \gamma_{D_2-x_2}\right) < \upsilon_2\right) \\ &= 1 - \Pr\left(\gamma_{S_{k*}R-x_2} > \upsilon_2, \gamma_{D_2-x_1} > \upsilon_2, \gamma_{D_2-x_2} > \upsilon_2\right) \\ &= 1 - \underbrace{\Pr\left(\gamma_{S_{k*}R-x_2} > \upsilon_2\right)}_{\nabla_1^{SC1}} \\ &\quad \times \underbrace{\Pr\left(\gamma_{D_2-x_1} > \upsilon_2, \gamma_{D_2-x_2} > \upsilon_2\right)}_{\nabla_2^{SC1}}. \end{aligned} \tag{16}$$

Proposition 2: It can be derived expression of outage probability at D_2 in closed-form as

$$\begin{aligned} &OP_2^{SC1} \\ &= 1 - \sum_{k=1}^{K} \binom{K}{k} (-1)^{k-1} \exp\left(-\frac{k\upsilon_2 N_0}{a_2 P_{BS}\lambda_{SR}}\right) \\ &\quad \times \sum_{n=1}^{N} \binom{N}{n} (-1)^{n-1} \sqrt{\frac{4n\theta\upsilon_2 N_0}{\xi\lambda_{BR}\lambda_{D2}}} K_1\left(\sqrt{\frac{4n\theta\upsilon_2 N_0}{\xi\lambda_{BR}\lambda_{D2}}}\right), \end{aligned} \tag{17}$$

where $\theta = \max\left(\frac{1}{(a_1 - \upsilon_1 a_2)}, \frac{1}{a_2}\right)$.

Proof: See Appendix B.

3) OUTAGE ANALYSIS AT D_2 WITH IMPERFECT SIC

When the imperfect SIC occurs, the SINR to decode x_2 at the link $S \to R$ is rewritten as

$$\gamma_{S_k Rip-x_2} = \frac{a_2 P_S \left|g_{S_k R}\right|^2}{a_1 P_S \left|\overline{g}_{S_k R}\right|^2 + N_0}. \tag{18}$$

The SINR to decode x_2 related to the link $R \to D_2$ is given by

$$\gamma_{D_2 ip-x_2} = \frac{a_2 P_R \left|g_{D_2}\right|^2}{a_1 P_R \left|\overline{g}_{D_2}\right|^2 + N_0}. \tag{19}$$

As a result, the outage probability at D_2 in imperfect SIC case is rewritten as

$$\begin{aligned} OP_{2ip}^{SC1} &= \Pr\left(\min\left(\gamma_{S_{k*}Rip-x_2}, \gamma_{D_2 ip-x_2}\right) < \upsilon_2\right) \\ &= 1 - \Pr\left(\gamma_{S_{k*}Rip-x_2} > \upsilon_2, \gamma_{D_2 ip-x_2} > \upsilon_2\right) \\ &= 1 - \underbrace{\Pr\left(\gamma_{S_{k*}Rip-x_2} > \upsilon_2\right)}_{\psi_1^{SC1}} \times \underbrace{\Pr\left(\gamma_{D_2 ip-x_2} > \upsilon_2\right)}_{\psi_2^{SC1}}. \end{aligned} \tag{20}$$

Proposition 3: The closed-form expression of outage probability in imperfect SIC case at D_2 is computed by

$$OP_{2ip}^{SC1} = 1 - \sum_{k=1}^{K}\sum_{m=1}^{K}\binom{K}{k}\binom{K}{m}(-1)^{k+m-2} \times \frac{ma_2\lambda_{SR}}{k\upsilon_2 a_1\lambda_{SRip} + ma_2\lambda_{SR}} \exp\left(-\frac{k\upsilon_2 N_0}{a_2 P_S \lambda_{SR}}\right) \times \sum_{n=1}^{N}\binom{N}{n}(-1)^{n-1}\frac{a_2\xi\lambda_{D2}}{\upsilon_2 a_1\xi\lambda_{D2ip} + a_2\xi\lambda_{D2}}. \quad (21)$$

Proof: See Appendix C.

B. ASYMPTOTIC ANALYSIS

In case of $P_S \to \infty$, the lower bound of outage probability for users D_1, D_2 (perfect SIC and imperfect SIC) are respectively given as

$$OP_{1-asym}^{SC1} = 1 - \sum_{n=1}^{N}\binom{N}{n}(-1)^{n-1}, \quad (22)$$

$$OP_{2-asym}^{SC1} = 1 - \sum_{n=1}^{N}\binom{N}{n}(-1)^{n-1}, \quad (23)$$

$$OP_{2ip-asym}^{SC1} = 1 - \sum_{k=1}^{K}\sum_{m=1}^{K}\binom{K}{k}\binom{K}{m}(-1)^{k+m-2} \times \frac{ma_2\lambda_{SR}}{k\upsilon_2 a_1\lambda_{SRip} + ma_2\lambda_{SR}} \times \sum_{n=1}^{N}\binom{N}{n}(-1)^{n-1}\frac{a_2\xi\lambda_{D2}}{\upsilon_2 a_1\xi\lambda_{D2ip} + a_2\xi\lambda_{D2}}. \quad (24)$$

Remark 2: Such asymptotic outage performance of users provides acceptable limitation of NOMA-MEC system. It is predicted that asymptotic expressions of outage probability result in a good matching with exact expressions of outage probability at specific range of SNR. We further verify these expectations in the section of numerical simulation.

Remark 3: From (22), (23) and (24), diversity order of the system under investigation equals zero. Therefore, these asymptotic expressions related outage performance are independent of transmit SNR at source. In particular, at high SNR, the outage performance will meet the outage floors. This observation is versified in the section of numerical simulation.

IV. SCHEME 2: ENERGY HARVESTING AT BOTH THE CAMERA AND THE RELAY

In the process of wireless power transfer, the operation of camera is limited by power source and hence harvested energy enables camera to prolong its lifetime. In this circumstance, the group of PBs still support both the camera and the relay with similar quality due to randomly selection of *PB* based on corresponding link's quality. This ability is possible as camera located close to the PBs.

The harvested energy at the camera S can written by

$$E_S = \tau P_B \alpha T \left|g_{B_{n*}S}\right|^2. \quad (25)$$

Under the assumption that the processing energy at S is negligible, the transmit power of S is given by

$$P_S = \frac{2\tau P_B \alpha \left|g_{B_{n*}S}\right|^2}{(1-\alpha)} = \xi\left|g_{B_{n*}S}\right|^2. \quad (26)$$

A. OUTAGE ANALYSIS

1) OUTAGE ANALYSIS AT D_1

The outage probability at D_1 in Scheme 2 is defined as

$$\begin{aligned} OP_1^{SC2} &= \Pr\left[\min\left(\gamma_{S_{k*}R-x_1}, \gamma_{D_1-x_1}\right) < \upsilon_1\right] \\ &= 1 - \Pr\left(\gamma_{S_{k*}R-x_1} > \upsilon_1, \gamma_{D_1-x_1} > \upsilon_1\right) \\ &= 1 - \underbrace{\Pr\left(\gamma_{S_{k*}R-x_1} > \upsilon_1\right)}_{\partial_1^{SC2}} \times \underbrace{\Pr\left(\gamma_{D_1-x_1} > \upsilon_1\right)}_{\partial_2^{SC1}}. \end{aligned} \quad (27)$$

Proposition 4: The outage probability of D_1 is computed in the closed-form expression as

$$\begin{aligned} OP_1^{SC2} = 1 &- \sum_{k=1}^{K}\sum_{n=1}^{N}\binom{K}{k}\binom{N}{n}(-1)^{k+n-2} \\ &\times \sqrt{\frac{4kn\upsilon_1 N_0}{(a_1 - \upsilon_1 a_2)\,\xi\lambda_{SR}\lambda_S}} K_1 \\ &\times \left(\sqrt{\frac{4kn\upsilon_1 N_0}{(a_1 - \upsilon_1 a_2)\,\xi\lambda_{SR}\lambda_{BS}}}\right) \\ &\times \sum_{n=1}^{N}\binom{N}{n}(-1)^{n-1}\sqrt{\frac{4n\upsilon_1 N_0}{\xi\,(a_1 - \upsilon_1 a_2)\,\lambda_{BR}\lambda_{D1}}} \\ &\times K_1\left(\sqrt{\frac{4n\upsilon_1 N_0}{\xi\,(a_1 - \upsilon_1 a_2)\,\lambda_{BR}\lambda_{D1}}}\right). \end{aligned} \quad (28)$$

Proof: See Appendix D.

2) OUTAGE ANALYSIS AT D_2 WITH PERFECT SIC

In case of perfect SIC, outage probability at the second MEC D_2 is formulated as

$$\begin{aligned} &OP_2^{SC2} \\ &= \Pr\left(\min\left(\gamma_{S_{k*}R-x_2}, \gamma_{D_2-x_1}, , \gamma_{D_2-x_2}\right) < \upsilon_2\right) \\ &= 1 - \Pr\left(\gamma_{S_{k*}R-x_2} > \upsilon_2, \gamma_{D_2-x_1} > \upsilon_2, \gamma_{D_2-x_2} > \upsilon_2\right) \\ &= 1 - \underbrace{\Pr\left(\gamma_{S_{k*}R-x_2} > \upsilon_2\right)}_{\nabla_1^{SC2}} \times \underbrace{\Pr\left(\gamma_{D_2-x_1} > \upsilon_2, \gamma_{D_2-x_2} > \upsilon_2\right)}_{\nabla_2^{SC1}}. \end{aligned} \quad (29)$$

Proposition 5: The closed-form expression for D_2 in case of perfect SIC is derived as

$$OP_2^{SC2} = 1 - \sum_{k=1}^{K}\sum_{n=1}^{N}\binom{K}{k}\binom{N}{n}(-1)^{k+n-2} \times \sqrt{\frac{4kn\upsilon_2 N_0}{a_2\xi\lambda_{SR}\lambda_{BS}}}K_1\left(\sqrt{\frac{4kn\upsilon_2 N_0}{a_2\xi\lambda_{SR}\lambda_{BS}}}\right) \times \sum_{n=1}^{N}\binom{N}{n}(-1)^{n-1}\sqrt{\frac{4n\theta\upsilon_2 N_0}{\xi\lambda_{BR}\lambda_{D2}}}K_1 \times \left(\sqrt{\frac{4n\theta\upsilon_2 N_0}{\xi\lambda_{BR}\lambda_{D2}}}\right). \quad (30)$$

Proof: See Appendix E.

3) OUTAGE ANALYSIS AT D_2 WITH IMPERFECT SIC

To indicate outage performance of D_2 with imperfect SIC in Scheme 2, we formulate outage probability as

$$\begin{aligned} OP_{2ip}^{SC2} &= \Pr\left(\min\left(\gamma_{S_{k*}Rip-x_2}, \gamma_{D_2ip-x_2}\right) < \upsilon_2\right) \\ &= 1 - \Pr\left(\gamma_{S_{k*}Rip-x_2} > \upsilon_2, \gamma_{D_2ip-x_2} > \upsilon_2\right) \\ &= 1 - \underbrace{\Pr\left(\gamma_{S_{k*}Rip-x_2} > \upsilon_2\right)}_{\psi_1^{SC2}} \times \underbrace{\Pr\left(\gamma_{D_2ip-x_2} > \upsilon_2\right)}_{\psi_2^{SC2}}. \end{aligned} \quad (31)$$

Proposition 6: The closed-form expression in imperfect SIC at D_2 is given as (32), shown in the bottom of the next page.

Proof: See Appendix F.

Remark 4: These results indicate that outage probability of NOMA-MEC which depends on various parameters. Firstly, fixed power allocation factor a_1, a_2 are set at the smart camera and they make outage difference among two MEC devices. The optimal outage performance with respect to a_1, a_2 is hard problem, it will be considered in future work. However, amount of harvested power P_B, P_S together with the number of transmit antennas at S and the number of power beacons are main reason to make outage behavior change significantly. Such analysis is further verified in numerical result.[4]

V. THE BENCHMARK OF OMA-MEC

In this section, OMA-MEC system is considered as a benchmark to highlight advantage of NOMA-MEC. In the first phase, the received signal at link $S \to R$ is given by

$$y_{S-R}^O = \sqrt{P_S}g_{S_kR}x_i + \omega_R, i \in \{1, 2\}. \quad (33)$$

In OMA-MEC mode, the SINR to decode x_i at R is given by

$$\gamma_{S_kR-x_i}^O = \frac{P_S\left|g_{S_kR}\right|^2}{N_0}. \quad (34)$$

[4]The problem of energy efficient is reported in [34], in which the time-switching factor related power beacon can be optimized to maximize by employing the Dinkelbach algorithm with Brent's method, together with the time-consuming exhaustive search approaches.

In the second phase, the received signal at D_i is given by

$$y_{R-D_i}^O = \sqrt{P_R}g_{D_i}x_i + \omega_{D_i}. \quad (35)$$

The SINR to decode x_i at D_i is given by

$$\gamma_{D_i-x_i}^O = \frac{P_R\left|g_{D_i}\right|^2}{N_0}. \quad (36)$$

In similar way, it can be found outage probability of OMA-MEC in Scheme 1 as

$$\begin{aligned} &OP_{SC1-i}^O \\ &= \Pr\left(\min\left(\gamma_{S_{k*}R-x_i}^O, \gamma_{D_i-x_i}^O\right) < \upsilon_i^O\right) \\ &= 1 - \Pr\left(\gamma_{S_{k*}R-x_i}^O > \upsilon_i^O\right)\Pr\left(\gamma_{D_i-x_i}^O > \upsilon_i^O\right) \\ &= 1 - \Pr\left(\left|g_{S_{k*}R}\right|^2 > \frac{\upsilon_i^O N_0}{P_S}\right)\Pr\left(\left|g_{B_{n*}R}\right|^2 > \frac{\upsilon_i^O N_0}{\xi\left|g_{D_i}\right|^2}\right) \\ &= 1 - \sum_{k=1}^{K}\sum_{n=1}^{N}\binom{K}{k}\binom{N}{n}(-1)^{k+n-2}\frac{1}{\lambda_{Di}} \times \exp\left(-\frac{k\upsilon_i^O N_0}{P_S\lambda_{SR}}\right)\int_0^\infty \exp\left(-\frac{n\upsilon_i^O N_0}{\xi x} - \frac{x}{\lambda_{Di}}\right)dx \\ &= 1 - \sum_{k=1}^{K}\sum_{n=1}^{N}\binom{K}{k}\binom{N}{n}(-1)^{k+n-2} \times \exp\left(-\frac{k\upsilon_i^O N_0}{P_S\lambda_{SR}}\right)\sqrt{\frac{4n\upsilon_i^O N_0}{\xi\lambda_{Di}}}K_1\left(\sqrt{\frac{4n\upsilon_i^O N_0}{\xi\lambda_{Di}}}\right), \end{aligned} \quad (37)$$

where $\upsilon_i^O = 2^{4R_i} - 1$.

In the scenario of both S and R are allowed to harvest energy from group of beacons, the outage event is formulated as

$$\begin{aligned} OP_{SC2-i}^O &= \Pr\left(\min\left(\gamma_{S_{k*}R-x_i}^O, \gamma_{D_i-x_i}^O\right) < \upsilon_i^O\right) \\ &= 1 - \Pr\left(\gamma_{S_{k*}R-x_i}^O > \upsilon_i^O, \gamma_{D_i-x_i}^O > \upsilon_i^O\right) \\ &= 1 - \underbrace{\Pr\left(\gamma_{S_{k*}R-x_i}^O > \upsilon_i^O\right)}_{\varpi_1} \times \underbrace{\Pr\left(\gamma_{D_i-x_i}^O > \upsilon_i^O\right)}_{\varpi_2}. \end{aligned} \quad (38)$$

Proposition 7: We can compute outage probability of OMA-MEC at D_i as

$$\begin{aligned} &OP_{SC2-i}^O \\ &= 1 - \sum_{k=1}^{K}\sum_{n=1}^{N}\binom{K}{k}\binom{N}{n}(-1)^{k+n-2} \times \sqrt{\frac{4knN_0\upsilon_i^O}{\xi\lambda_{SR}\lambda_{BS}}}K_1\left(\sqrt{\frac{4knN_0\upsilon_i^O}{\xi\lambda_{SR}\lambda_{BS}}}\right) \times \sum_{n=1}^{N}\binom{N}{n}(-1)^{n-1}\sqrt{\frac{4n\upsilon_i^O N_0}{\xi\lambda_{Di}\lambda_{BR}}}K_1\left(\sqrt{\frac{4n\upsilon_i^O N_0}{\xi\lambda_{Di}\lambda_{BR}}}\right). \end{aligned} \quad (39)$$

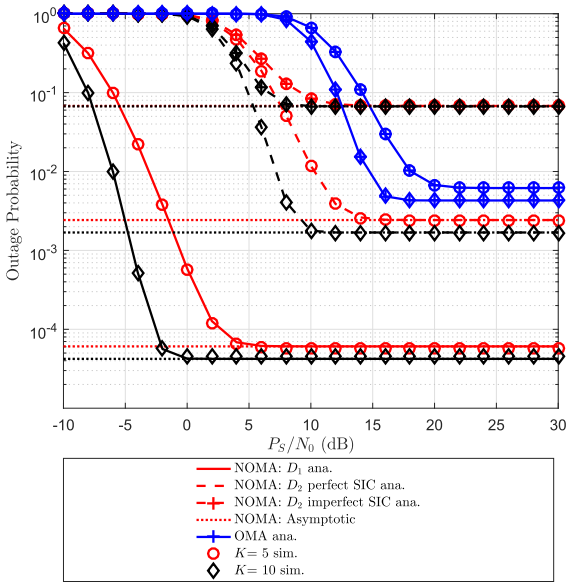

FIGURE 3. Scheme 1: Comparison study on outage probability of NOMA and OMA versus P_S/N_0 as changing $K = N$ ($a_1 = 0.7$, $P_B/N_0 = 30$ (dB)).

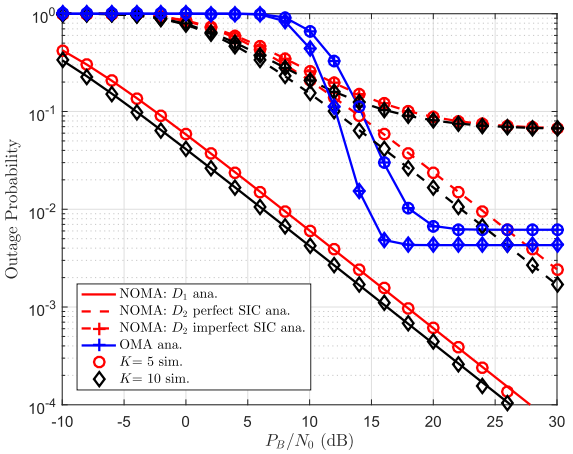

FIGURE 4. Scheme 1: Comparison study on outage probability of NOMA and OMA versus P_B/N_0 as changing $K = N$ ($a_1 = 0.7$, $P_S/N_0 = 30$ (dB)).

Proof: We omit the proof due to similarity as previous propositions.

VI. SIMULATION RESULTS

In this section, we perform simulations to evaluate the performance of the proposed IoT system. We first reveal the outage performance of the first scheme in which energy harvesting is enabled at only relay R. Then the simulation results are used to provided comparison between two schemes. This paper only presents main metric, i.e. outage probability. We omit the throughput performance metric here since it can be achieved straightforward manner. In these simulations, we set the number of antennas at S is same as the number of beacons $K = N = 3$ except for specific cases. The other parameters are given, such as target rates $R_1 = 0.5$ (bps/Hz), $R_2 = 2$ (bps/Hz), channel gains $\lambda_{BS} = \lambda_{BR} = 1, \lambda_{SR} = \lambda_{D1} = 10, \lambda_{D2} = 5, \lambda_{SRip} = \lambda_{D2ip} = 0.01$, coefficients related to energy harvesting $\tau = 0.8, \alpha = 0.6$ except for specific cases.

Fig. 3 demonstrates the outage performance of the considered system in Scheme 1 versus transmit SNR at S in the uplink NOMA-MEC system. For outage comparison, the outage performance of D_1 is better than that of D_2 which depends on performance of SIC. The main reason is that higher power allocation factor a_1 associated with D_1. It can be seen clearly that D_2 in perfect SIC provides better outage performance than that in imperfect SIC case. Moreover, asymptotic lines match with analytical curves at high region of transmit SNR at the smart camera S. This is predicted as Remark 3. Such situation confirmed the exactness of our derived asymptotic expressions. In addition, this figure compares two cases ($K = 5, 10$) of antenna configuration at S. Since S is equipped more antennas, it can be observed that lower outage probability occurs at $K = 10$. It is also proved that analytical results are matched with numerical results. Fig. 4 depicts similar trends as Fig. 3; however varying transmit SNR at the PB makes the proposed system in OMA with $K = 10$ meets saturation early than other curves. This can be explained by diversity order equaling zero.

Fig. 5 indicates significant impact of power allocation factors on system performance of D_1, D_2 versus target rates required at MEC devices. It confirms that performance gaps of each device with two cases $a_1 = 0.8, a_1 = 0.9$ can be seen clearly in entire range of target rates. We set $P_S/N_0 = 40$ (dB), $P_B/N_0 = 10$ (dB). This illustration allows system to adjust factor a_1 to achieve fairness among two MEC devices.

It need be further examined impact of amount of harvested energy on outage performance versus energy efficiency factor τ at S as in Fig. 6. Comparing outage performance of two MEC devices with two cases $P_S/N_0 = 10$ (dB), $P_S/N_0 = 20$ (dB), small gap exists in the base station D_1 and D_2 with perfect SIC. By increasing τ, the outage performance changes slightly. It can be explained that there exists saturated threshold for harvested power at the relay R related to outage performance.

$$OP_{2ip}^{SC2} = 1 - \sum_{k=1}^{K}\sum_{m=1}^{K}\sum_{n=1}^{N}\binom{K}{k}\binom{K}{m}\binom{N}{n}(-1)^{k+m+n-3}\frac{ma_2\lambda_{SR}}{k\upsilon_2 a_1\lambda_{SRip} + ma_2\lambda_{SR}}\sqrt{\frac{4kn\upsilon_2 N_0}{a_2\xi\lambda_{SR}\lambda_{BS}}}K_1\left(\sqrt{\frac{4kn\upsilon_2 N_0}{a_2\xi\lambda_{SR}\lambda_{BS}}}\right)$$
$$\times \sum_{n=1}^{N}\binom{N}{n}(-1)^{n-1}\frac{a_2\xi\lambda_{D2}}{\upsilon_2 a_1\xi\lambda_{D2ip} + a_2\xi\lambda_{D2}}\sqrt{\frac{4n\upsilon_2 N_0}{a_2\xi\lambda_{D2}\lambda_{BR}}}K_1\left(\sqrt{\frac{4n\upsilon_2 N_0}{a_2\xi\lambda_{D2}\lambda_{BR}}}\right). \quad (32)$$

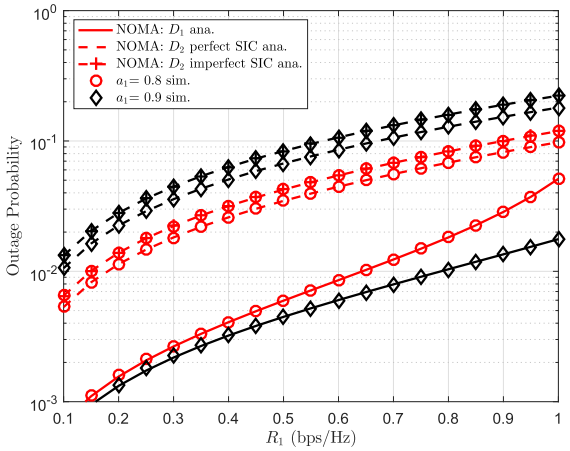

FIGURE 5. Scheme 1: Comparison study on outage probability of NOMA versus target rates $R_1 = R_2$ as changing a_1.

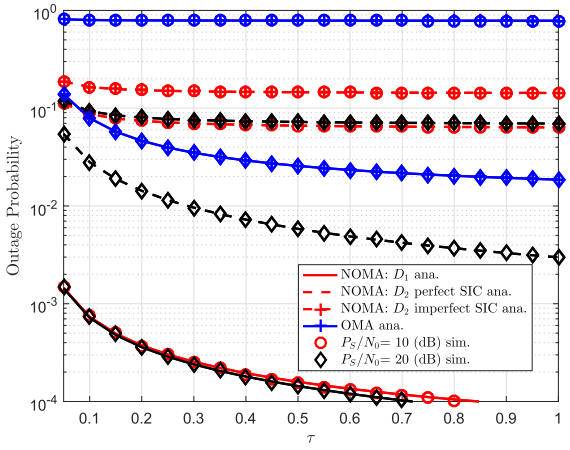

FIGURE 6. Scheme 1: Comparison study on outage probability of NOMA and OMA versus τ as changing P_S ($a_1 = 0.7, P_B/N_0 = 30$ (dB)).

It can be observed the improvement of outage performance of Scheme 2 for two devices by enhance quality of wireless channel as in Fig. 7. The stronger channels of two links, i.e. link the selected PB to S, link the selected PB to relay make influence on outage behavior of D_1, D_2. This observation provides the guidelines to locate the group beacon close to both the smart camera and the relay to achieve better performance. Although small amount of harvested energy is bewared, but strong wireless powered channels contribute to enhance outage behavior of two devices. It should be balance between benefits of energy harvesting and ability of signal processing.

Fig. 8 compares outage performance of two schemes. Interestingly, although the smart camera S harvests energy to serve for its uplink to MEC, outage performance corresponds to Scheme 2 is still slightly better than that of Scheme 1 once P_B/N_0 is greater than 20 (dB). That can be explained by higher power facilitated to PBs benefits to the proposed system in two schemes. Two schemes exhibit the same performance at low region of P_B/N_0 and $P_S/N_0 = 10$ (dB). This observation confirms such NOMA-MEC still benefits from

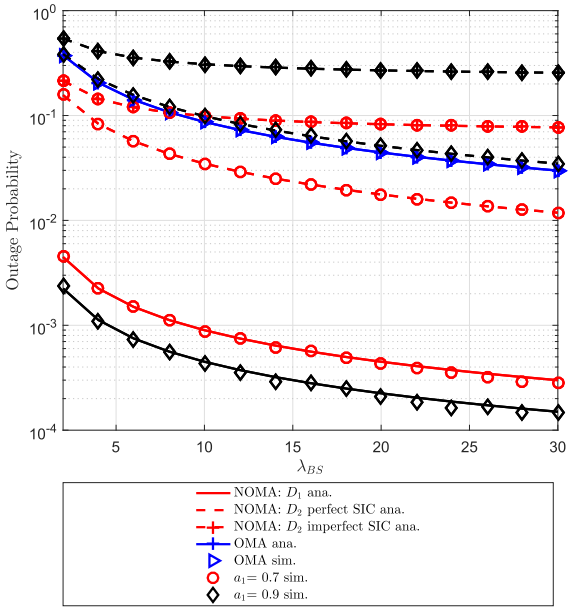

FIGURE 7. Scheme 2: Outage performance versus $\lambda_{BS} = \lambda_{BR}$ as changing a_1 ($P_B/N_0 = 30$ (dB)).

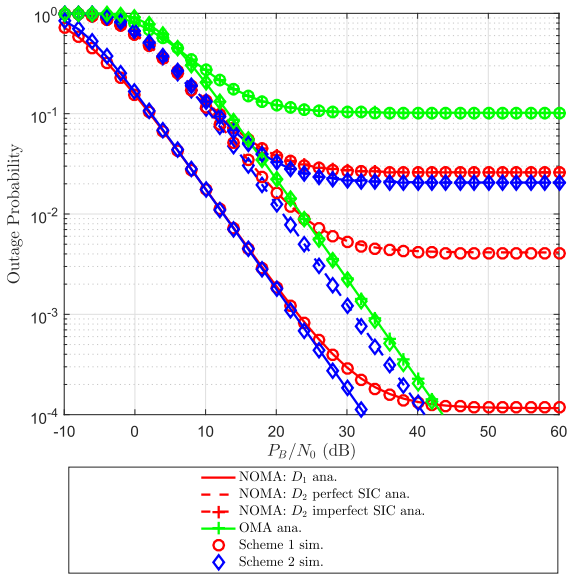

FIGURE 8. Comparison study on outage probability of Scheme 1 and Scheme 2 versus P_B/N_0 ($P_S/N_0 = 10$ (dB), $K = N = 3$).

energy harvesting to improve operation of sensors with limited power resource. The distance between the power beacon and sensor nodes is key factor to improve outage performance since energy efficiency is very limited in current technology of circuit [34].

VII. CONCLUSION

In this paper, we proposed a uplink for NOMA-enabled MEC system operating under ability of energy harvesting from the group of PBs. We derive exact closed-form expression of outage probability for each signal at MEC associated with the base stations. In addition, we examined two scenarios

of opportunity of energy harvesting from the relay or the source, which was compared in term of outage performance sequentially. It was shown that the proposed system provides NOMA-enabled MEC with better outage performance than OMA-enabled MEC. In addition, the outage improvement can be obtained since more antennas equipped at the camera (sensor) in such IoT system and more PBs are activated. As a future work, optimal user pairing algorithms for NOMA-enabled MEC system will be considered under multi-MEC scenario.

APPENDIX

APPENDIX A

PROOF OF PROPOSITION 1

From (10) and (14), ∂_1^{SC1} can be computed by

$$\begin{aligned}\partial_1^{SC1} &= \Pr\left(\gamma_{S_{k*}R-x_1} > \upsilon_1\right)\\ &= \Pr\left(\left|g_{S_{k*}R}\right|^2 > \frac{\upsilon_1 N_0}{P_S\left(a_1-\upsilon_1 a_2\right)}\right)\\ &= \sum_{k=1}^{K}\binom{K}{k}(-1)^{k-1}\exp\left(-\frac{k\upsilon_1 N_0}{P_S\left(a_1-\upsilon_1 a_2\right)\lambda_{SR}}\right).\end{aligned} \tag{A.1}$$

From (11) and (14), ∂_2^{SC1} can be computed by (A.2), as shown at the bottom of the next page where the last equation can be achieved from the fact that $\int_0^\infty \exp\left(-\frac{\delta}{4x}-\varphi x\right)dx = \sqrt{\frac{\delta}{\varphi}}K_1\left(\sqrt{\delta\varphi}\right)$ in [40, Eq. (3.352.4)].

Replacing (A.1), (A.2) into (14), it completes the proof.

APPENDIX B

PROOF OF PROPOSITION 2

From (10) and (16), ∇_1^{SC1} can be expressed by

$$\begin{aligned}\nabla_1^{SC1} &= \Pr\left(\gamma_{S_{k*}R-x_2} > \upsilon_2\right)\\ &= \Pr\left(\left|g_{S_{k*}R}\right|^2 > \frac{\upsilon_2 N_0}{a_2 P_S}\right)\\ &= \sum_{k=1}^{K}\binom{K}{k}(-1)^{k-1}\exp\left(-\frac{k\upsilon_2 N_0}{a_2 P_S\lambda_{SR}}\right).\end{aligned} \tag{B.1}$$

Next, ∇_2^{SC1} can be computed from result in (16) as

$$\begin{aligned}\nabla_2^{SC1} &= \Pr\left(\gamma_{D_2-x_1} > \upsilon_2, \gamma_{D_2-x_2} > \upsilon_2\right)\\ &= \Pr\left(\left|g_{B_{n*}R}\right|^2 > \frac{\upsilon_2 N_0}{\xi\left(a_1-\upsilon_2 a_2\right)\left|g_{D_2}\right|^2}, \left|g_{B_{n*}R}\right|^2 > \frac{\upsilon_2 N_0}{a_2\xi\left|g_{D_2}\right|^2}\right)\\ &= \Pr\left(\left|g_{B_{n*}R}\right|^2 > \frac{\theta\upsilon_2 N_0}{\xi\left|g_{D_2}\right|^2}\right)\\ &= \int_0^\infty\left(1-F_{\left|g_{B_{n*}R}\right|^2}\left(\frac{\theta\upsilon_2 N_0}{\xi x}\right)\right)f_{\left|g_{D_2}\right|^2}(x)\,dx.\end{aligned} \tag{B.2}$$

From (10) and (11), by exploiting related CDF and PDF, ∇_2^{SC1} is further computed by

$$\begin{aligned}\nabla_2^{SC1} &= \sum_{n=1}^{N}\binom{N}{n}(-1)^{n-1}\frac{1}{\lambda_{D2}}\\ &\quad\times\int_0^\infty\exp\left(-\frac{n\theta\upsilon_2 N_0}{\xi\lambda_{BR}x}-\frac{x}{\lambda_{D2}}\right)dx\\ &= \sum_{n=1}^{N}\binom{N}{n}(-1)^{n-1}\sqrt{\frac{4n\theta\upsilon_2 N_0}{\xi\lambda_{BR}\lambda_{D2}}}\\ &\quad\times K_1\left(\sqrt{\frac{4n\theta\upsilon_2 N_0}{\xi\lambda_{BR}\lambda_{D2}}}\right).\end{aligned} \tag{B.3}$$

Plugging (B.1), (B.3) into (16), the final result can be obtained as in Proposition 2.

It is the end of the proof.

APPENDIX C

PROOF OF PROPOSITION 3

From (10) and (20), we can express ψ_1^{SC1} as

$$\begin{aligned}&\psi_1^{SC1}\\ &= \Pr\left(\gamma_{S_{k*}Rip-x_2} > \upsilon_2\right)\\ &= \Pr\left(\left|g_{S_{k*}R}\right|^2 > \frac{\upsilon_2\left(a_1 P_S\left|\overline{g}_{S_{k*}R}\right|^2+N_0\right)}{a_2 P_S}\right)\\ &= \int_0^\infty\left(1-F_{\left|g_{S_{k*}R}\right|^2}\left(\frac{\upsilon_2\left(a_1 P_S x+N_0\right)}{a_2 P_S}\right)\right)f_{\left|\overline{g}_{S_{k*}R}\right|^2}(x)\,dx.\end{aligned} \tag{C.1}$$

By exploiting related CDF and PDF, ψ_1^{SC1} is further computed by

$$\begin{aligned}\psi_1^{SC1} &= \sum_{k=1}^{K}\sum_{m=1}^{K}\binom{K}{k}\binom{K}{m}(-1)^{k+m-2}\frac{m}{\lambda_{SRip}}\\ &\quad\times\exp\left(-\frac{k\upsilon_2 N_0}{a_2 P_S\lambda_{SR}}\right)\\ &\quad\times\int_0^\infty\exp\left(-\left(\frac{k\upsilon_2 a_1}{a_2\lambda_{SR}}+\frac{m}{\lambda_{SRip}}\right)x\right)dx\\ &= \sum_{k=1}^{K}\sum_{m=1}^{K}\binom{K}{k}\binom{K}{m}(-1)^{k+m-2}\\ &\quad\times\frac{m a_2\lambda_{SR}}{k\upsilon_2 a_1\lambda_{SRip}+m a_2\lambda_{SR}}\exp\left(-\frac{k\upsilon_2 N_0}{a_2 P_S\lambda_{SR}}\right).\end{aligned} \tag{C.2}$$

From (20), ψ_2^{SC1} can be rewritten as

$$\begin{aligned}\psi_2^{SC1} &= \Pr\left(\gamma_{D_2 ip-x_2} > \upsilon_2\right)\\ &= \Pr\left(\frac{a_2\xi\left|g_{B_{n*}R}\right|^2\left|g_{D_2}\right|^2}{a_1\xi\left|g_{B_{n*}R}\right|^2\left|\overline{g}_{D_2}\right|^2+N_0} > \upsilon_2\right)\\ &= \Pr\left(\left|g_{D_2}\right|^2 > \frac{\upsilon_2\left(a_1\xi\left|g_{B_{n*}R}\right|^2\left|\overline{g}_{D_2}\right|^2+N_0\right)}{a_2\xi\left|g_{B_{n*}R}\right|^2}\right)\\ &= \int_0^\infty\int_0^\infty\left(1-F_{\left|g_{D_2}\right|^2}\left(\frac{\upsilon_2\left(a_1\xi xy+N_0\right)}{a_2\xi x}\right)\right)\\ &\quad\times f_{\left|g_{B_{n*}R}\right|^2}(x)\,dx f_{\left|\overline{g}_{D_2}\right|^2}(y)\,dy. \qquad (C.3)\end{aligned}$$

In similar way, ψ_2^{SC1} is formulated by (C.4), as shown at the top of the next page

The expected result can be obtained by plugging (C.2), (C.3), into (20).

It is the end of the proof.

APPENDIX D
PROOF OF PROPOSITION 4

With the help of (25), ∂_1^{SC2} can be expressed by

$$\begin{aligned}\partial_1^{SC2} &= \Pr\left(\gamma_{S_{k*}R-x_1} > \upsilon_1\right)\\ &= \Pr\left(\left|g_{S_{k*}R}\right|^2 > \frac{\upsilon_1 N_0}{\left(a_1-\upsilon_1 a_2\right)\xi\left|g_{B_{n*}S}\right|^2}\right)\\ &= \int_0^\infty\left(1-F_{\left|g_{S_{k*}R}\right|^2}\left(\frac{\upsilon_1 N_0}{\left(a_1-\upsilon_1 a_2\right)\xi x}\right)\right)\\ &\quad\times f_{\left|g_{B_{n*}S}\right|^2}(x)\,dx\\ &= \sum_{k=1}^{K}\sum_{n=1}^{N}\binom{K}{k}\binom{N}{n}(-1)^{k+n-2}\frac{n}{\lambda_{BS}}\\ &\quad\times\int_0^\infty\exp\left(-\frac{k\upsilon_1 N_0}{\left(a_1-\upsilon_1 a_2\right)\xi\lambda_{SR}x}-\frac{nx}{\lambda_{BS}}\right)dx\\ &= \sum_{k=1}^{K}\sum_{n=1}^{N}\binom{K}{k}\binom{N}{n}(-1)^{k+n-2}\\ &\quad\times\sqrt{\frac{4kn\upsilon_1 N_0}{\left(a_1-\upsilon_1 a_2\right)\xi\lambda_{SR}\lambda_{BS}}}\\ &\quad\times K_1\left(\sqrt{\frac{4kn\upsilon_1 N_0}{\left(a_1-\upsilon_1 a_2\right)\xi\lambda_{SR}\lambda_{BS}}}\right). \qquad (D.1)\end{aligned}$$

Plugging (A.2), (D.1), into (25), the final result can be obtained as in Proposition 4.

It is the end of the proof.

APPENDIX E
PROOF OF PROPOSITION 5

From (27), ∇_1^{SC2} can be computed by

$$\begin{aligned}\nabla_1^{SC2} &= \Pr\left(\gamma_{S_{k*}R-x_2} > \upsilon_2\right)\\ &= \Pr\left(\left|g_{S_{k*}R}\right|^2 > \frac{\upsilon_2 N_0}{a_2\xi\left|g_{B_{n*}S}\right|^2}\right)\\ &= \int_0^\infty\left(1-F_{\left|g_{S_{k*}R}\right|^2}\left(\frac{\upsilon_2 N_0}{a_2\xi\left|g_{B_{n*}S}\right|^2}\right)\right)f_{\left|g_{B_{n*}S}\right|^2}(x)\,dx\\ &= \sum_{k=1}^{K}\sum_{n=1}^{N}\binom{K}{k}\binom{N}{n}(-1)^{k+n-2}\frac{n}{\lambda_{BS}}\\ &\quad\times\int_0^\infty\exp\left(-\frac{k\upsilon_2 N_0}{a_2\xi\lambda_{SR}x}-\frac{nx}{\lambda_{BS}}\right)dx\\ &= \sum_{k=1}^{K}\sum_{n=1}^{N}\binom{K}{k}\binom{N}{n}(-1)^{k+n-2}\\ &\quad\times\sqrt{\frac{4kn\upsilon_2 N_0}{a_2\xi\lambda_{SR}\lambda_{BS}}}K_1\left(\sqrt{\frac{4kn\upsilon_2 N_0}{a_2\xi\lambda_{SR}\lambda_{BS}}}\right). \qquad (E.1)\end{aligned}$$

Plugging (B.3), (E.1), into (25), the result in Proposition 5 is obtained.

It is the end of the proof.

APPENDIX F
PROOF OF PROPOSITION 6

From (29), ψ_1^{SC2} can be computed by (F.1) as the top of the next page.

ψ_2^{SC2} can be computed by (F.2) as the top of the next page.

$$\begin{aligned}\partial_2^{SC1} &= \Pr\left(\gamma_{D_1-x_1} > \upsilon_1\right)\\ &= \Pr\left(\left|g_{D_1}\right|^2 > \frac{\upsilon_1 N_0}{\left|g_{B_{n*}R}\right|^2\xi\left(a_1-\upsilon_1 a_2\right)}\right)\\ &= \int_0^\infty\left(1-F_{\left|g_{D_1}\right|^2}\left(\frac{\upsilon_1 N_0}{x\xi\left(a_1-\upsilon_1 a_2\right)}\right)\right)f_{\left|g_{B_{n*}R}\right|^2}(x)\,dx\\ &= \sum_{n=1}^{N}\binom{N}{n}(-1)^{n-1}\frac{n}{\lambda_{BR}}\int_0^\infty\exp\left(-\frac{\upsilon_1 N_0}{\xi\left(a_1-\upsilon_1 a_2\right)\lambda_{D1}x}-\frac{nx}{\lambda_{BR}}\right)dx\\ &= \sum_{n=1}^{N}\binom{N}{n}(-1)^{n-1}\sqrt{\frac{4n\upsilon_1 N_0}{\xi\left(a_1-\upsilon_1 a_2\right)\lambda_{BR}\lambda_{D1}}}K_1\left(\sqrt{\frac{4n\upsilon_1 N_0}{\xi\left(a_1-\upsilon_1 a_2\right)\lambda_{BR}\lambda_{D1}}}\right), \qquad (A.2)\end{aligned}$$

$$\psi_2^{SC1} = \sum_{n=1}^{N}\binom{N}{n}(-1)^{n-1}\frac{n}{\lambda_{BR}}\frac{1}{\lambda_{D2ip}}\int_0^\infty\int_0^\infty \exp\left(-\frac{\upsilon_2 a_1\xi y}{a_2\xi\lambda_{D2}}-\frac{\upsilon_2 N_0}{a_2\xi\lambda_{D2}x}\right)\exp\left(-\frac{nx}{\lambda_{BR}}\right)dx\exp\left(-\frac{y}{\lambda_{D2ip}}\right)dy$$
$$= \sum_{n=1}^{N}\binom{N}{n}(-1)^{n-1}\frac{n}{\lambda_{BR}}\frac{1}{\lambda_{D2ip}}\int_0^\infty \exp\left(-\left(\frac{\upsilon_2 a_1\xi}{a_2\xi\lambda_{D2}}+\frac{1}{\lambda_{D2ip}}\right)y\right)dy\int_0^\infty \exp\left(-\frac{\upsilon_2 N_0}{a_2\xi\lambda_{D2}x}-\frac{nx}{\lambda_{BR}}\right)dx$$
$$= \sum_{n=1}^{N}\binom{N}{n}(-1)^{n-1}\frac{a_2\xi\lambda_{D2}}{\upsilon_2 a_1\xi\lambda_{D2ip}+a_2\xi\lambda_{D2}}\sqrt{\frac{4n\upsilon_2 N_0}{a_2\xi\lambda_{D2}\lambda_{BR}}}K_1\left(\sqrt{\frac{4n\upsilon_2 N_0}{a_2\xi\lambda_{D2}\lambda_{BR}}}\right). \tag{C.4}$$

$$\psi_1^{SC2} = \Pr\left(\gamma_{S_{k*}Rip-x_2} > \upsilon_2\right)$$
$$= \Pr\left(\frac{a_2\xi\left|g_{B_{n*}S}\right|^2\left|g_{S_{k*}R}\right|^2}{a_1\xi\left|g_{B_{n*}S}\right|^2\left|\overline{g}_{S_{k*}R}\right|^2+N_0} > \upsilon_2\right)$$
$$= \Pr\left(\left|g_{S_{k*}R}\right|^2 > \frac{\upsilon_2 a_1\left|\overline{g}_{S_{k*}R}\right|^2}{a_2}+\frac{\upsilon_2 N_0}{a_2\xi\left|g_{B_{n*}S}\right|^2}\right)$$
$$= \int_0^\infty\int_0^\infty\left(1-F_{\left|g_{S_{k*}R}\right|^2}\left(\frac{\upsilon_2 a_1 x}{a_2}+\frac{\upsilon_2 N_0}{a_2\xi y}\right)\right)f_{\left|\overline{g}_{S_{k*}R}\right|^2}(x)\,f_{\left|g_{B_{n*}S}\right|^2}(y)\,dxdy$$
$$= \sum_{k=1}^{K}\sum_{m=1}^{K}\sum_{n=1}^{N}\binom{K}{k}\binom{K}{m}\binom{N}{n}(-1)^{k+m+n-3}\frac{m}{\lambda_{SRip}}\frac{n}{\lambda_{BS}}\int_0^\infty \exp\left(-\frac{k\upsilon_2 a_1 x}{a_2\lambda_{SR}}-\frac{mx}{\lambda_{SRip}}\right)dx$$
$$\int_0^\infty \exp\left(-\frac{k\upsilon_2 N_0}{a_2\xi\lambda_{SR}y}-\frac{ny}{\lambda_{BS}}\right)dy$$
$$= \sum_{k=1}^{K}\sum_{m=1}^{K}\sum_{n=1}^{N}\binom{K}{k}\binom{K}{m}\binom{N}{n}(-1)^{k+m+n-3}\frac{ma_2\lambda_{SR}}{k\upsilon_2 a_1\lambda_{SRip}+ma_2\lambda_{SR}}\sqrt{\frac{4kn\upsilon_2 N_0}{a_2\xi\lambda_{SR}\lambda_{BS}}}K_1\left(\sqrt{\frac{4kn\upsilon_2 N_0}{a_2\xi\lambda_{SR}\lambda_{BS}}}\right). \tag{F.1}$$

$$\psi_2^{SC2} = \Pr\left(\gamma_{D_2ip-x_2} > \upsilon_2\right)$$
$$= \Pr\left(\frac{a_2\xi\left|g_{B_{n*}R}\right|^2\left|g_{D_2}\right|^2}{a_1\xi\left|g_{B_{n*}R}\right|^2\left|\overline{g}_{D_2}\right|^2+N_0} > \upsilon_2\right)$$
$$= \Pr\left(\left|g_{D_2}\right|^2 > \frac{\upsilon_2\left(a_1\xi\left|g_{B_{n*}R}\right|^2\left|\overline{g}_{D_2}\right|^2+N_0\right)}{a_2\xi\left|g_{B_{n*}R}\right|^2}\right)$$
$$= \int_0^\infty\int_0^\infty\left(1-F_{\left|g_{D_2}\right|^2}\left(\frac{\upsilon_2\left(a_1\xi xy+N_0\right)}{a_2\xi x}\right)\right)f_{\left|g_{B_{n*}R}\right|^2}(x)\,dx f_{\left|\overline{g}_{D_2}\right|^2}(y)\,dy$$
$$= \sum_{n=1}^{N}\binom{N}{n}(-1)^{n-1}\frac{n}{\lambda_{BR}}\frac{1}{\lambda_{D2ip}}\int_0^\infty \exp\left(-\left(\frac{\upsilon_2 a_1\xi}{a_2\xi\lambda_{D2}}+\frac{1}{\lambda_{D2ip}}\right)y\right)dy\int_0^\infty \exp\left(-\frac{\upsilon_2 N_0}{a_2\xi\lambda_{D2}x}-\frac{nx}{\lambda_{BR}}\right)dx$$
$$= \sum_{n=1}^{N}\binom{N}{n}(-1)^{n-1}\frac{a_2\xi\lambda_{D2}}{\upsilon_2 a_1\xi\lambda_{D2ip}+a_2\xi\lambda_{D2}}\sqrt{\frac{4n\upsilon_2 N_0}{a_2\xi\lambda_{D2}\lambda_{BR}}}K_1\left(\sqrt{\frac{4n\upsilon_2 N_0}{a_2\xi\lambda_{D2}\lambda_{BR}}}\right). \tag{F.2}$$

Plugging (F.1), (F.2) into (29), the final result can be obtained as in Proposition 6.

It is the end of the proof.

REFERENCES

[1] A. Al-Fuqaha, M. Guizani, M. Mohammadi, M. Aledhari, and M. Ayyash, "Internet of Things: A survey on enabling technologies, protocols, and spplications," *IEEE Commun. Surveys Tuts.*, vol. 17, no. 4, pp. 2347–2376, 4th Quart., 2015.

[2] R. Zhang, M. Wang, X. Shen, and L.-L. Xie, "Probabilistic analysis on QoS provisioning for Internet of Things in LTE–A heterogeneous networks with partial spectrum usage," *IEEE Internet Things J.*, vol. 3, no. 3, pp. 354–365, Jun. 2016.

[3] N. Abbas, Y. Zhang, A. Taherkordi, and T. Skeie, "Mobile edge computing: A survey," *IEEE Internet Things J.*, vol. 5, no. 1, pp. 450–465, Feb. 2018.

[4] D. Wang, B. Bai, K. Lei, W. Zhao, Y. Yang, and Z. Han, "Enhancing information security via physical layer approaches in heterogeneous IoT with multiple access mobile edge computing in smart city," *IEEE Access*, vol. 7, pp. 54508–54521, 2019.

[5] M. Min, L. Xiao, Y. Chen, P. Cheng, D. Wu, and W. Zhuang, "Learning-based computation offloading for IoT devices with energy harvesting," *IEEE Trans. Veh. Technol.*, vol. 68, no. 2, pp. 1930–1941, Feb. 2019.

[6] F. Wang, J. Xu, X. Wang, and S. Cui, "Joint offloading and computing optimization in wireless powered mobile-edge computing systems," in *Proc. IEEE Int. Conf. Commun. (ICC)*, Paris, France, May 2017, pp. 1–6.

[7] Y. Lu, C. Cheng, J. Yang, and G. Gui, "Improved Hybrid Precoding Scheme for mmWave Large-Scale MIMO Systems," *IEEE Access*, vol. 7, pp. 12027–12034, 2019.
[8] L. Song, Y. Li, Z. Ding, and H. V. Poor, "Resource management in non-orthogonal multiple access networks for 5G and beyond," *IEEE Netw.*, vol. 31, no. 4, pp. 8–14, Jul. 2017.
[9] K. A. Remley *et al.*, "Measurement challenges for 5G and beyond: An update from the national Institute of standards and technology," *IEEE Microw. Mag.*, vol. 18, no. 5, pp. 41–56, Jul./Aug. 2017.
[10] N. Zhang, P. Yang, J. Ren, D. Chen, L. Yu, and X. Shen, "Synergy of big data and 5G wireless networks: Opportunities, approaches, and challenges," *IEEE Wireless Commun.*, vol. 25, no. 1, pp. 12–18, Feb. 2018.
[11] F. Tang, Z. M. Fadlullah, B. Mao, and N. Kato, "An intelligent traffic load prediction-based adaptive channel assignment algorithm in SDN-IoT: A deep learning approach," *IEEE Internet Things J.*, vol. 5, no. 6, pp. 5141–5154, Dec. 2018.
[12] F. Tang, B. Mao, Z. M. Fadlullah, and N. Kato, "On a novel deep-learning-based intelligent partially overlapping channel assignment in SDN-IoT," *IEEE Commun. Mag.*, vol. 56, no. 9, pp. 80–86, Sep. 2018.
[13] J. Ni, X. Lin, and X. S. Shen, "Efficient and secure service-oriented authentication supporting network slicing for 5G-enabled IoT," *IEEE J. Sel. Areas Commun.*, vol. 36, no. 3, pp. 644–657, Mar. 2018.
[14] D.-T. Do, A.-T. Le, C.-B. Le and B. M. Lee, "On exact outage and throughput performance of cognitive radio based non-orthogonal multiple access networks with and without D2D link," *Sensors*, vol. 19, no. 15, p. 3314, 2019.
[15] D.-T. Do, M. Vaezi, and T.-L. Nguyen, "Wireless powered cooperative relaying using NOMA with imperfect CSI," in *Proc. IEEE Globecom Workshops (GC Wkshps)*, Abu Dhabi, UAE, Dec. 2018, pp. 1–6.
[16] D.-T. Do, A.-T. Le, and A. B. M. Lee, "On performance analysis of underlay cognitive radio-aware hybrid OMA/NOMA networks with imperfect CSI," *Electronics*, vol. 8, no. 7, p. 819, Jul. 2019.
[17] P. D. Diamantoulakis, K. N. Pappi, Z. Ding, and G. K. Karagiannidis, "Wireless-powered communications with non-orthogonal multiple access," *IEEE Trans. Wireless Commun.*, vol. 15, no. 12, pp. 8422–8436, Dec. 2016.
[18] H. Chingoska, Z. Hadzi-Velkov, I. Nikoloska, and N. Zlatanov, "Resource allocation in wireless powered communication networks with non-orthogonal multiple access," *IEEE Wireless Commun. Lett.*, vol. 5, no. 6, pp. 684–687, Dec. 2016.
[19] M. Song and M. Zheng, "Energy efficiency optimization for wireless powered sensor networks with nonorthogonal multiple access," *IEEE Sensors Lett.*, vol. 2, no. 1, pp. 1–4, Mar. 2018.
[20] M. Moltafet, P. Azmi, N. Mokari, M. R. Javan, and A. Mokdad, "Optimal and fair energy efficient resource allocation for energy harvesting-enabled-PD-NOMA-based HetNets," *IEEE Trans. Wireless Commun.*, vol. 17, no. 3, pp. 2054–2067, Mar. 2018.
[21] Y. Wang, Y. Wu, F. Zhou, Z. Chu, Y. Wu, and F. Yuan, "Multi-objective resource allocation in a NOMA cognitive radio network with a practical non-linear energy harvesting model," *IEEE Access*, vol. 6, pp. 12973–12982, 2018.
[22] Z. Yang, Y. Pan, W. Xu, R. Guan, Y. Wang, and M. Chen, "Energy efficient resource allocation for machine-to-machine communications with NOMA and energy harvesting," in *Proc. IEEE Conf. Comput. Commun. Workshops*, Atlanta, GA, USA, May 2017, pp. 145–150.
[23] Z. Yang, W. Xu, Y. Pan, C. Pan, and M. Chen, "Energy efficient resource allocation in machine-to-machine communications with multiple access and energy harvesting for IoT," *IEEE Internet Things J.*, vol. 5, no. 1, pp. 229–245, Feb. 2018.
[24] D.-T. Do and M.-S. Van Nguyen, "Device-to-device transmission modes in NOMA network with and without wireless power transfer," *Comput. Commun.*, vol. 139, pp. 67–77, May 2019.
[25] T.-L. Nguyen and D.-T. Do, "Exploiting impacts of intercell interference on SWIPT-assisted non-orthogonal multiple access," *Wireless Commun. Mobile Comput.*, vol. 2018, pp. 1–12, Nov. 2018, Art. no. 2525492.
[26] X. Li, M. Huang, C. Zhang, D. Deng, K. M. Rabie, Y. Ding, and J. Du, "Security and reliability performance analysis of cooperative multi-relay systems with nonlinear energy harvesters and hardware impairments," *IEEE Access*, vol. 7, pp. 102644–102661, 2019.
[27] F. Zhou, H. Sun, Z. Chu, and R. Q. Hu, "Computation efficiency maximization for wireless-powered mobile edge computing," in *Proc. IEEE Global Commun. Conf. (GLOBECOM)*, Abu Dhabi, United Arab Emirates, Dec. 2018, pp. 1–6.
[28] X. Zhang, Y. Wang, F. Zhou, N. Al-Dhahir, and X. Deng, "Robust resource allocation for MISO cognitive radio networks under two practical non-linear energy harvesting models," *IEEE Commun. Lett.*, vol. 22, no. 9, pp. 1874–1877, Sep. 2018.
[29] F. Zhou, Z. Chu, H. Sun, R. Q. Hu, and L. Hanzo, "Artificial noise aided secure cognitive beamforming for cooperative MISO-NOMA using SWIPT," *IEEE J. Sel. Areas Commun.*, vol. 36, no. 4, pp. 918–931, Apr. 2018.
[30] M. Ashraf, A. Shahid, J. W. Jang, and K.-G. Lee, "Energy harvesting non-orthogonal multiple access system with multi-antenna relay and base station," *IEEE Access*, vol. 5, pp. 17660–17670, 2017.
[31] W. Han, J. Ge, and J. Men, "Performance analysis for NOMA energy harvesting relaying networks with transmit antenna selection and maximal-ratio combining over Nakagami-m fading," *IET Commun.*, vol. 10, no. 18, pp. 2687–2693, Dec. 2016.
[32] X. Wang, Z. Na, K.-Y. Lam, X. Liu, Z. Gao, F. Li, and L. Wang, "Energy efficiency optimization for NOMA-based cognitive radio with energy harvesting," *IEEE Access*, vol. 7, pp. 139172–139180, 2019.
[33] S. K. Zaidi, S. F. Hasan, and X. Gui, "Evaluating the ergodic rate in SWIPT-aided hybrid NOMA," *IEEE Commun. Lett.*, vol. 22, no. 9, pp. 1870–1873, Sep. 2018.
[34] Y. Wang, W. Yang, X. Shang, J. Hu, Y. Huang, and Y. Cai, "Energy-efficient secure transmission for wireless powered Internet of Things with multiple power beacons," *IEEE Access*, vol. 6, pp. 75086–75098, 2018.
[35] S. Lee, D. Benevides da Costa, and T. Q. Duong, "Outage probability of non-orthogonal multiple access schemes with partial relay selection," in *Proc. IEEE 27th Annu. Int. Symp. Pers., Indoor, Mobile Radio Commun.*, Valencia, Spain, Sep. 2016, pp. 4–8.
[36] Z. Ding, H. Dai, and H. V. Poor, "Relay selection for cooperative NOMA," *IEEE Wireless Commun. Lett.*, vol. 5, no. 4, pp. 416–419, Aug. 2016.
[37] N.-P. Nguyen, T. Q. Duong, H. Q. Ngo, Z. Hadzi-Velkov, and L. Shu, "Secure 5G wireless communications: A joint relay selection and wireless power transfer approach," *IEEE Access*, vol. 4, pp. 3349–3359, 2016.
[38] A. A. Nasir, X. Zhou, S. Durrani, and R. A. Kennedy, "Relaying protocols for wireless energy harvesting and information processing," *IEEE Trans. Wireless Commun.*, vol. 12, no. 7, pp. 3622–3636, Jul. 2013.
[39] S. Arzykulov, T. A. Tsiftsis, G. Nauryzbayev, M. Abdallah, and G. Yang, "Outage performance of underlay CR-NOMA networks with Detect-and-Forward relaying," in *Proc. IEEE Global Commun. Conf. (GLOBECOM)*, Dec. 2018, pp. 1–6.
[40] I. S. Gradshteyn and I. M. Ryzhik, *Table of Integrals, Series, and Products*, 7th ed. San Diego, CA, USA: Academic, 2007.

DINH-THUAN DO (Senior Member, IEEE) received the B.S., M.Eng., and Ph.D. degrees in communications engineering from Viet Nam National University (VNU-HCM), in 2003, 2007, and 2013, respectively. From 2003 to 2009, he was a Senior Engineer with VinaPhone Mobile Network. From 2009 to 2010, he was a Visiting Ph.D. Student with the Communications Engineering Institute, National Tsing Hua University, Taiwan. He published over 75 SCI/SCIE journal articles and one sole author book, five book chapters. His research interests include signal processing in wireless communications network, cooperative communications, non-orthogonal multiple access, full-duplex transmission, and energy harvesting. He was a recipient of the Golden Globe Award from Vietnam Ministry of Science and Technology, in 2015 (Top ten excellent young scientists nationwide). He is a lead Guest Editor in Special Issue titled Recent Advances for 5G: Emerging Scheme of NOMA in Cognitive Radio and Satellite Communications Electronics, 2019, and a Guest Editor in Special Issue titled Massive Sensors Data Fusion for Health-Care Informatics in Annals of Telecommunications, 2020. He is currently serving as an Associate Editor in six journals, in which main journals are *Eurasip Journal on Wirelesss Communications and Networking*, *Computer Communications (Elservier)*, *Electronics*, and *KSII Transactions on Internet and Information Systems*.

MINH-SANG VAN NGUYEN was born in Bentre, Vietnam. He is currently pursuing the master's degree in wireless communications. He has worked with the Industrial University of Ho Chi Minh City, Vietnam. His research interests include electronic design, signal processing in wireless communications networks, non-orthogonal multiple access, and physical layer security.

TU N. NGUYEN (Senior Member, IEEE) received the Ph.D. degree in electronic engineering from the National Kaohsiung University of Science and Technology (formerly, National Kaohsiung University of Applied Sciences), Kaohsiung, Taiwan, in 2016. He joined the Intelligent Systems Center, Missouri University of Science and Technology, as a Postdoctoral Researcher, in 2016. He was a Postdoctoral Associate with the Department of Computer Science and Engineering, University of Minnesota- Twin Cities, in 2017. He is currently an Assistant Professor with the Department of Computer Science, Purdue University at Fort Wayne, Fort Wayne, IN, USA. His research interests include design and analysis of algorithms, network science, cyberphysical systems, and cybersecurity. He was also a technical program committee member for more than 70 premium conferences in the areas of network and communication, such as INFOCOM, Globecom, ICC, and RFID. He was a TPC Co-Chair of the NAFOSTED Conference on Information and Computer Science (NICS) 2019, SoftCOM (25th), and EAI International Conference on Context-Aware Systems and Applications (ICCASA) 2017. He was a Publicity Chair of the International Conference on Awareness Science and Technology (iCAST) 2017 and BigDataSecurity 2017. He was a Track Chair for ACT 2017. Since 2017, he has been an Associate Editor of IEEE Access and *EURASIP Journal on Wireless Communications and Networking*. He is also on the Editorial Board of *Cybersecurity* journal, *Internet Technology Letters*, since 2017, the *International Journal of Vehicle Information and Communication Systems*, since 2017, the *International Journal of Intelligent Systems Design and Computing*, since 2017, and *IET Wireless Sensor Systems*, since 2017.

XINGWANG LI (Senior Member, IEEE) received the B.Sc. degree from Henan Polytechnic University, in 2007, the M.Sc. degree from the University of Electronic Science and Technology of China, in 2010, and the Ph.D. degree from the Beijing University of Posts and Telecommunications, in 2015. From 2010 to 2012, he was working as an Engineer with Comba Telecom Ltd., in Guangzhou, China. From 2016 to 2018, he was also a Visiting Scholar with the State Key Laboratory of Networking and Switching Technology, Beijing University of Posts and Telecommunications. From 2017 to 2018, he was a Visiting Scholar with Queen's University Belfast, Belfast, U.K. He is currently an Associate Professor with the School of Physics and Electronic Information Engineering, Henan Polytechnic University, Jiaozuo, China. His research interests include MIMO communication, cooperative communication, hardware constrained communication, non-orthogonal multiple access, physical layer security, unmanned aerial vehicles, and the Internet-of-Things. He has served as many TPC members, such as the IEEE/CIC International Conference on Communications in China (ICCC'2019) and the IEEE Global Communications Conference 2018 (Globecom'18). He is also an Editor on the Editorial Board of IEEE Access, *Computer Communications*, and *KSII Transactions on Internet and Information Systems*.

KWONHUE CHOI received the B.S., M.S., and Ph.D. degrees in electronic and electrical engineering from the Pohang University of Science and Technology, Pohang, South Korea, in 1994, 1996, and 2000, respectively. From 2000 to 2003, he was a Senior Research Staff Member with the Electronics and Telecommunications Research Institute, Daejeon, South Korea. He joined the Department of Information and Communication Engineering, Yeungnam University, Gyeongsan, South Korea, in 2003, where he is currently a Professor. He has authored a text book *Problem-Based Learning in Communication Systems Using MATLAB and Simulink* (Wiley, 2016). His research interests include signal design for the communication systems, multiple access schemes, diversity schemes for wireless fading channels, and multiple antenna systems.